INORGANIC CHEMISTRY
FRONTIERS

RESEARCH ARTICLE

View Article Online
View Journal | View Issue

Cite this: *Inorg. Chem. Front.*, 2023, **10**, 7319

2-Formylphenoxyacetic acid Schiff bases: a promising ligand scaffold for readily available trigonal prismatic Co(II) single-ion magnets†

Kamil Kotrle, [a] Ivan Nemec, [a] Peter Antal,[a] Kamila Petrželová, [a] Erik Čižmár [b] and Radovan Herchel *[a]

This article presents a series of six mononuclear Co(II) complexes **1–6** featuring ligands derived from a hexadentate Schiff base family, originating from the condensation of (2-formylphenoxy)acetic acid with various diamines. Notably, these complexes uniquely prefer a trigonal prism geometry, presenting a novel approach to synthesizing complexes with this distinctive shape. The compounds were characterized by elemental analysis, FT-IR spectroscopy, and single-crystal and powder XRD techniques. Furthermore, the magnetism was investigated by DC and AC magnetic measurements and also complemented by X-band EPR spectroscopy. The results reveal that the prepared complexes behave as field-induced single-molecule magnets, characterized by a substantial negative axial zero-field splitting D-parameter and spin reversal energetic barrier U_{eff} reaching values up to 72 K. The theoretical methods based on CASSCF/NEVPT2 calculations were applied to rationalize their magnetic properties. Moreover, these complexes hold promising potential for further functionalization, offering opportunities to enhance their properties, particularly towards developing zero-field single-molecule magnets as evidenced by the slow relaxation of magnetization in zero static magnetic field observed for the zinc-diluted complex **1Zn**.

Received 23rd August 2023,
Accepted 26th October 2023

DOI: 10.1039/d3qi01691a

rsc.li/frontiers-inorganic

Introduction

In recent years, there has been significant development in the field of single-molecule magnets (SMMs), a class of materials that exhibit intriguing magnetic properties, including magnetic hysteresis and slow relaxation of magnetization at the molecular level. This progress began with discovering and studying these effects in large manganese polynuclear clusters, such as the renowned Mn12ac.[1] Subsequent research has explored a wide range of systems, with one notable subclass of SMMs known as single-ion magnets. These magnets consist of only one paramagnetic ion,[2] thereby minimizing the influence of any magnetic exchange interactions. Among this class of compounds, an important group, particularly within the first transition metals row, comprises complexes containing Co(II) as the central ion. Co(II) exhibits interesting magnetic properties due to its spin $S = 3/2$, making it a Kramers ion, and its relatively large spin–orbit coupling resulting from its occupation of the d-orbital.[3]

Although leveraging spin–orbit coupling is key to designing single-molecule magnets with significant magnetic anisotropy, another crucial characteristic of 3d single ion magnets is ligand field splitting, which is usually stronger than spin–orbit coupling.

In six-coordinated Co(II) complexes, the orbital contribution is usually substantial due to the nature of the ground state, which is T_{1g} for an octahedron (O_h), and $^4E'$ for a trigonal prism (D_{3h}). It is common for the (pseudo)octahedral symmetry to result in large and positive values of the axial zero-field splitting parameter D.[4] Positive D-parameter frequently leads to the easy-plane type anisotropy, and only significant rhombicity (E/D ratio) can provide the axial type anisotropy.[5] In the case of trigonal prism symmetry, the D-parameter is typically large and negative.[4] The relationship between the D-parameter and magnetic anisotropy barrier for half-integer spin complexes, such as Co(II), is defined as:[6]

$$U_{eff} = |D|\left(S^2 - \frac{1}{4}\right) \quad (1)$$

It is worth noting that a significant number of complexes with a trigonal prismatic shape exhibit slow relaxation of magnetization even in the absence of an external magnetic field, earning them the designation of zero-field SMMs. Table 1 lists

[a]*Department of Inorganic Chemistry, Faculty of Science, Palacký University, 17. listopadu 12, CZ-771 46 Olomouc, Czech Republic. E-mail: radovan.herchel@upol.cz*
[b]*Institute of Physics, Faculty of Science, P.J. Šafárik University in Košice, Park Angelinum 9, SK-041 54 Košice, Slovakia*

† Electronic supplementary information (ESI) available. CCDC 2288033–2288038. For ESI and crystallographic data in CIF or other electronic format see DOI: https://doi.org/10.1039/d3qi01691a

notable examples of trigonal prismatic and trigonally distorted hexacoordinate complexes showing the slow relaxation of magnetization.

It is evident that focusing on the design of Co(II) complexes as potential candidates for SMMs holds intriguing possibilities, including the potential for zero-field single-molecule magnets. However, such magnets are still relatively rare among Co(II) complexes as a whole due to the common occurrence of quantum tunneling of magnetization in the ground state. In the case of six-coordinated Co(II) complexes, the pseudo-octahedral shape is the most commonly observed coordination polyhedron. Therefore, efforts must be made to achieve the trigonal prism shape. Various strategies have already been applied as can be observed in Table 1. An effective approach, seen in most cases,[8–13] involves the use of three heterocyclic binding sites, each with two donor atoms, designed to prevent distortion and maintain the desired shape. In another instance,[14] the trigonal prismatic shape is achieved through bridging oxygen atoms in a tetranuclear core, where Co(II) is surrounded by three diamagnetic Co(III) cores. In the last case,[15] the desired shape is attained through steric hindrance caused by neocuproine methyl groups.

This work presents a series of six complexes (Scheme 1) that employ Schiff base ligands with similar structural motifs. These ligands induce a distorted coordination environment, compelling the Co(II) complexes to adopt shapes that closely resemble trigonal prismatic geometry. The ligands are derived from (2-formylphenoxy)acetic acid, and by incorporating different diamines, we observed a modulation of both the structural and magnetic properties. While analogous structures have been reported previously for Ni(II), Cu(II), Zn(II), and even Co(II), their magnetic properties have not been studied in detail.[16–20]

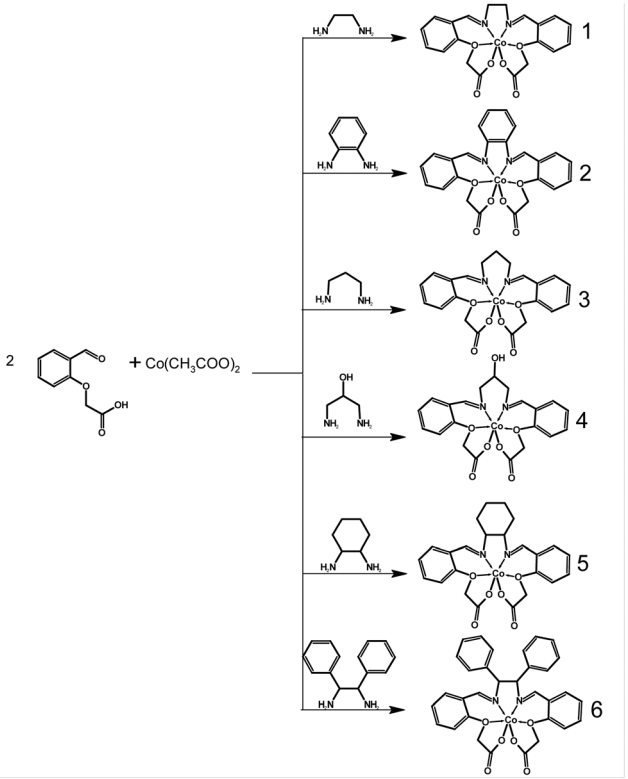

Scheme 1 General scheme for the synthesis of Co(II) complexes [CoL] of **1–6** with respective *in situ* prepared Schiff base ligands H_2L.

Results and discussion

Synthesis and characterisation

The methods employed for the preparation of these complexes are described in the Experimental section below. The Co(II) compounds **1–6** were synthesized by reacting a mixture of cobalt(II) acetate and (2-formylphenoxy)acetic acid with the corresponding amine.

Among these complexes, all except for **2** exhibit good solubility in methanol (MeOH); however, only complex **1** yielded a crystalline product from this solvent. As **3**, **5**, and **6** did not crystallize from methanol due to their high solubility, a mixture of propanol and methanol was chosen as the solvent. For insoluble complex **2**, crystals were obtained from dimethyl-

Table 1 Selected trigonal prismatic and trigonally distorted hexacoordinate Co(II) single-molecule magnets with magnetic parameters and continuous shape measures (CSM) deviations from ideal D_{3h} trigonal prismatic and O_h octahedral geometries *via* SHAPE software[7]

Name	D (cm^{-1})	E (cm^{-1})	U_{eff} (cm^{-1})	τ_0 (s)	B (T)	CSM TP	CSM OH	Ref.
$[Co(tppm)][BPh_4]_2$	−97.2(2)	$9.3(1) \times 10^{-3}$	192	$2.6(2) \times 10^{-12}$	0	0.554	15.893	8
$[Co(hpy)][BPh_4]_2 \cdot 3CH_2Cl_2$	−107.5(4)	3.5(3)	20	$1.2(1) \times 10^{-3}$	0	2.471	8.237	8
$[Co(PzOx)_3(BC_6H_5)]Cl \cdot CHCl_3$	−82	0.246	152	2.07×10^{-9}	0	0.828	16.272	9
$[Co(AcimOx)_3(BC_6H_5)]ClO_4$	−102.5		101	2.56×10^{-6}	0	0.905	13.462	10
$[Co(AcPyOx)_3BC_6H_5]ClO_4$	−86		194.6	3.55×10^{-10}	0	2.006	10.042	11
$\{Na[(Chdc)Co]\}(BPh_4)_3$	−75.8	9.1×10^{-4}	52.6		0.1	1.793	9.293	12
$[Co(tppm)][ClO_4]_2 \cdot 2CH_3CN \cdot H_2O$	−80.7	0.6	39.2	1.7×10^{-4}	0	0.588	14.920	13
$(HNEt_3)[Co^{II}Co^{III}_3(hpmp)_6]$	−115	2.8	76.3	1×10^{-7}	0	2.341	9.284	14
$[Co(neo)(CH_3COO)_2]$			26.3	1.361×10^{-7}	0.1	3.761	11.893	15
$[Co(neo)(piv)_2]$			13.2	6.2×10^{-6}	0.1	9.801	7.650	15
$[Co(neo)(4OH\text{-}benz)_2] \cdot 2CH_3OH$			12.2	1.04×10^{-6}	0.1	10.110	6.352	15

tppm = 6,6′,6″-(methoxymethanetriyl)tris(2-(1*H*-pyrazol-1-yl)pyridine); hpy = tris(2,2′-bipyrid-6-yl)methanol; PzOx = pyrazoloximate, AcimOx = acetylmethylimidazole-oximate, AcPyOx – acetylmethylpyridine-oximate, Chdc – 6,6′-{cyclohexane-1,3,5-diyltris[nitrilo(*E*)methylylidene]} dipyridine-3-carboxamide; H_2hpmp = *R*-4-bromo-2-((2-hydroxy-1-phenylethylimino)methyl)phenol; neo = neocuproine, piv = pivalate, 4OH-benz = 4-hydroxybenzoate.

sulfoxide (DMSO). Complex **3** presented a challenge during its preparation, as it often resulted in the formation of orange powder. Ultimately, this problem was resolved by conducting the reaction without heating the solution to the reflux temperature. Unfortunately, complex **4** could not be obtained in the required quantity and purity for bulk characterization due to the formation of undesired byproducts. However, a small number of single crystals of complex **4** were successfully prepared, and its structure was determined through X-ray analysis. This allowed us to characterize complex **4** at least with theoretical methods. The composition of the prepared complexes was verified through elemental analysis, infrared spectrometry (Fig. S1†), and X-ray powder diffraction (Fig. S2†). For complex **6**, X-ray crystallography indicated the presence of co-crystallized methanol solvent molecules, which displayed notable disorder, likely stemming from solvent loss during the experiment. It was not possible to model the solvent molecules properly and a solvent masking procedure was applied.[21] The resultant masked electron density corresponded to 1.25 methanol molecules per complex molecule. Of note here is that the single crystal measured had been promptly transferred from the solution to high viscosity oil. This action very likely contributed to the reduced rate of solvent loss. Thus, the observed alignment between the outcomes of elemental analysis and the assumption of a solvent-free complex is unsurprising.

Magnetically diluted complex **1Zn** was prepared by using Co(II) and Zn(II) acetate in a 1 : 9 molar ratio. Sample purity was verified by PXRD (Fig. S2†) and CHNS elemental analysis. The composition was studied by the AAS method, which showed a mass fraction of Co of 0.32%, which means that the diluted sample has formula $C_{21}H_{22}N_2O_7Co_{0.026}Zn_{0.974}$.

Crystal structure description

Complexes **1**, **4**, and **5** crystallize in the monoclinic space group $P2_1/n$, while **2** and **3** crystallize in the triclinic space group $P\bar{1}$. Complex **6** crystallizes in the orthorhombic space group *Iba*2. All diffraction experiments were conducted at room temperature. Each compound consists of a [CoL] neutral complex accompanied by co-crystallized solvent molecules of MeOH in the case of **1**, **3**, **4**, and **5**, and DMSO in the case of **2**. In each complex, the cobalt atom is bonded to four oxygen atoms and two nitrogen atoms. Notably, complexes **5** and **6** contain two symmetrically inequivalent molecules of the complex [CoL] in the asymmetric unit, labeled **5a**/**6a** and **5b**/**6b**, respectively (Fig. 1). Additional details about X-ray crystallographic experiments are listed in Table S1.†

The shape of the cobalt coordination polyhedron in all complex molecules is closest to a trigonal prism (D_{3h}), as confirmed by calculations of continuous shape measures (CSMs) using SHAPE software.[7] The minimal distortion pathway between a trigonal prism and an octahedron, as well as the deviation of the prepared complexes' structures from the pathway, is shown in Fig. S3.† It is apparent that all complexes exhibit significant deviations from an octahedron (O_h), except

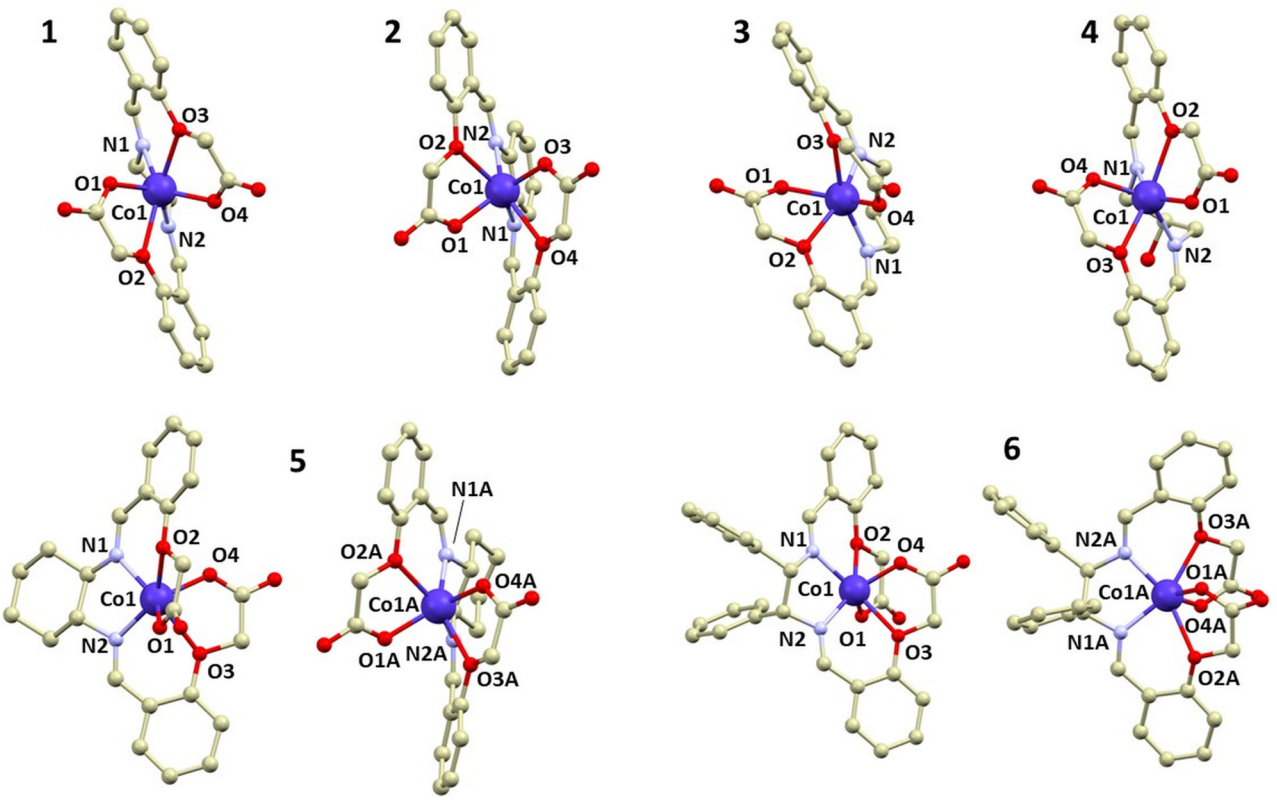

Fig. 1 A perspective view of the crystal structures of **1–6**, with hydrogen atoms omitted for the sake of clarity.

for **3**, which is nearly on the border between an octahedron and a trigonal prism.

In addition to CSM, the shape of the geometry of the coordination environment was also investigated using the newly proposed structural parameter τ_6, a geometry index ranging from 0 (ideal octahedron) to 1 (ideal trigonal prismatic shape).[22] This index is analogous to previously published τ_5 and τ_4 indices for penta- and tetracoordinate complexes, respectively.[23] The parameter τ_6 is defined as

$$\tau_6 = \frac{540 - (\alpha + \beta + \gamma)}{150} \quad (2)$$

with the help of three angles α, β and γ, which are the three greatest valence angles of the coordination center. Index τ_6 shows that all prepared complexes are closer to trigonal prismatic than to octahedral geometry (Table 2). These results seem to correlate well with CSM analysis (Fig. S4†), showing **1** and **5a** as the closest to the trigonal prism, from the studied series.

Furthermore, a previously known similar complex, [Co(fapapn)]·6H_2O (CSD code HOMFOF),[17] was included in the SHAPE analysis, which is a conformational isomer to **3** and exhibits a structure much closer to an ideal octahedron. Interestingly, the use of different solvents (HOMFOF synthesis used a mixture of ethanol and water) for synthesis results in entirely different structures, which are expected to possess distinct properties, especially from a magnetic standpoint.

The distances between the metal and ligand donor atoms, as listed in Table 2, reveal that in most cases, the four bonds between the central atoms and the Schiff base N-atoms or carboxylic group O-atoms have very similar lengths ranging between 2.0 and 2.1 Å. However, the bonds between Co and the etheric group O-atoms (O2 and O3) are longer, ranging between 2.2 and 2.4 Å. Furthermore, structures that differ from others in terms of their shape (CSM), such as **3** and its isomer with the CSD code HOMFOF, do not appear to differ significantly in their bond lengths, except for a shorter distance between the Co atom and the etheric O atom in the HOMFOF structure.

Complexes **1–5** crystallize as crystal solvates, with dimethyl sulfoxide as the solvent in structure **2**, and methanol in all other cases. Methanol is bound to the complex molecule through a hydrogen bond. In structures **1**, **4**, and **5**, it is bound to the carboxylic group oxygen, which is not connected to the central cobalt atom. In structure **3**, methanol is bound to the coordinating carboxylic oxygen atom. Moreover, structure **4** contains a ligand with a hydroxyl group, which forms a hydrogen bond with the carboxyl group oxygen, resulting in a supramolecular structure mediated by hydrogen bridges. Details about observed significant hydrogen bonds are shown in the ESI (Fig. S5†).

Magnetic measurements

DC magnetic measurements were conducted for compounds **1–3** and **5–6**. The measurements consisted of recording the magnetization as a function of temperature under a magnetic field of 0.2 T and as a function of the magnetic field (Fig. 2) at temperatures of 1.8, 5, and 10 K (or 2 and 5 K for compound **1**).

The effective magnetic moments of the prepared compounds at a temperature limit of 300 K are as follows: 4.79μ_B for compound **1**, 5.15μ_B for compound **2**, 4.55μ_B for compound **3**, 5.13μ_B for compound **5**, and 4.83μ_B for compound **6**.

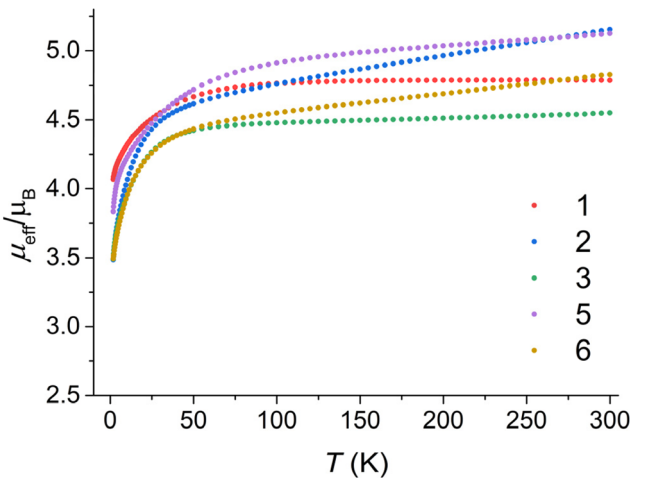

Fig. 2 The effective magnetic moment dependence on temperature for all studied compounds **1–3** and **5–6**.

Table 2 Selected bond distances (Å) and CSM deviations from ideal trigonal prism and octahedron for complexes **1–6**

	Co–N1	Co–N2	Co–O1	Co–O2	Co–O3	Co–O4	CSM TP	CSM OH	τ_6
1	2.0829(19)	2.0736(18)	1.9911(14)	2.3176(14)	2.2822(15)	1.9848(16)	1.631	16.812	0.802
2	2.0883(13)	2.0681(13)	1.9922(12)	2.2846(12)	2.2688(11)	1.9759(12)	1.882	13.748	0.777
3	2.0770(15)	2.0929(15)	2.0370(13)	2.2257(13)	2.2451(13)	2.0110(13)	4.727	5.626	0.525
4	2.130(2)	2.092(2)	1.983(2)	2.335(2)	2.299(2)	1.993(1)	1.481	12.924	0.794
5a	2.0667(19)	2.0739(19)	1.9861(17)	2.2963(15)	2.3525(15)	1.9879(16)	1.911	17.842	0.802
5b[a]	2.083(2)	2.081(2)	1.9946(17)	2.2755(18)	2.2164(16)	2.0099(18)	1.472	12.663	0.785
6a	2.066(6)	2.107(8)	1.951(5)	2.336(5)	2.383(5)	1.970(7)	2.612	18.154	0.760
6b[a]	2.052(6)	2.065(8)	1.998(5)	2.399(6)	2.375(5)	1.978(6)	4.714	15.726	0.694
	Co–N1	Co–N2	Co–O1	Co–O3	Co–O4	Co–O5			
HOMFOF[b]	2.063(2)	2.055(2)	2.042(2)	2.192(2)	2.184(2)	2.032(2)	10.644	1.530	0.320

[a] N1 and N2 for these structures are marked as N3 and N4 in Fig. 1. Same way, O1–O4 are marked as O7–O10. [b] Labeled in a similar way as in Fig. 1, in the HOMFOF cif file, N1 is N1, N2 is N2, O1 is O1, O2 is O3, O3 is O4 and O4 is O5.

The spin-only value for $S = 3/2$ with $g = 2.0$ is $3.87\mu_B$. The observed larger values of the magnetic moment can be attributed to an increased g-factor resulting from orbital contribution and temperature-independent paramagnetism.[24]

DC magnetic data were analyzed using the following spin Hamiltonian:

$$\hat{H} = D(\hat{S}_z{}^2 - \hat{S}^2/3) + E(\hat{S}_x{}^2 - \hat{S}_y{}^2) + \mu_B B g \hat{S} \quad (3)$$

The best-fitted spin Hamiltonian parameters are listed in Table 3 with the standard deviations listed in Table S2,† and calculated magnetic data compared to the experimental ones are depicted in Fig. S6–S10.†

For complexes **5** and **6**, the fits neglected the inclusion of two symmetrically inequivalent molecules in the asymmetric unit. Instead, the fits were performed to obtain the same parameters for both molecules in order to prevent over-parameterization of the fit. In the case of complex **6**, a positive D-parameter was used in the fit, which was suggested by theoretical calculations for one of its symmetrically inequivalent molecules.

AC susceptibility measurements were performed on compounds **1–3** and **5–6** in the presence of a static magnetic field of 0.15 T (0.1 T for **1**), because the tunneling of the magnetization was too fast to observe the out-of-phase signal of AC susceptibility at zero static magnetic field. Under such circumstances, all the measured complexes exhibited out-of-phase signals, indicating the presence of field-induced slow relaxation of magnetization. For the fitting of the AC in-phase and out-of-phase susceptibilities, the Havriliak–Negami model was used[25]

$$\chi(\omega) = \chi_S + \frac{\chi_T - \chi_S}{(1 + (i\omega\tau)^{1-\alpha})^{\beta}} \quad (4)$$

This model is also derived for two relaxation processes:

$$\chi(\omega) = \chi_{S_1} + \frac{\chi_{T_1} - \chi_{S_1}}{(1 + (i\omega\tau_1)^{1-\alpha_1})^{\beta_1}} + \chi_{S_2} + \frac{\chi_{T_2} - \chi_{S_2}}{(1 + (i\omega\tau_2)^{1-\alpha_2})^{\beta_2}} \quad (5)$$

where χ_S and χ_T are adiabatic and isothermic parts of magnetic susceptibility, α and β are parameters describing peak asymmetry and broadness. When two processes are considered, the model is usually simplified with $\chi_{S1} = \chi_{S2}$. However, for certain complexes, simplified variants of this model were employed, such as the Cole–Davidson model ($\alpha = 0$), Cole–Cole model ($\beta = 1$), or Debye model ($\alpha = 0$; $\beta = 1$). Further information regarding the fit parameters can be found in Tables S3–S7.†

For complexes **1**, **2**, and **5**, the inspection of the Argand (Cole–Cole) plot revealed the presence of two relaxation processes. Consequently, the experimental AC data were fitted by considering this observation. Subsequently, the temperature dependence of the relaxation times was analyzed using the following equation:

$$\tau^{-1} = A_{dir} T H^{n_{dir}} + C_{Ram} T^{n_{Ram}} + \tau_0^{-1} e^{\frac{-U_{eff}}{T}} \quad (6)$$

where the direct, Raman, and Orbach relaxation mechanisms are involved. Exponential coefficients were fixed to agree with the theoretical values ($n_{dir} = 4$, $n_{Ram} = 5$).[26] Results are shown in Fig. 3 for **1**, and for the rest of the compounds in Fig. S11–S16.† Complex **6** did not exhibit an observable maximum of out-of-phase susceptibility within the measured frequency range; hence, further analysis was not conducted for this complex. The results for the remaining complexes are provided in Table 4.

In the case of complexes **1** and **2**, only a small range of temperatures (2.2 K–2.6 K for **1** and 2.8 K–3.0 K for **2**) exhibited two clearly distinguishable processes that could be fitted.

Table 3 The best-fitted parameters according to spin Hamiltonian (eqn (1)) for compounds **1–3** and **5–6**

	g^a	D (cm^{-1})	E/D	TIP (cm^3 mol^{-1})
1	2.724; 2.299	−30.3	0.173	0
2	2.344	−13.2	0.281	2.55×10^{-3}
3	2.357; 2.271	−17.0	0.195	3.34×10^{-4}
5	2.641; 2.395	−30.5	0.207	1.33×10^{-3}
6	2.148; 2.326	15.5	0.274	1.67×10^{-3}

[a] Written either as g_{iso}, or g_z; g_{xy}.

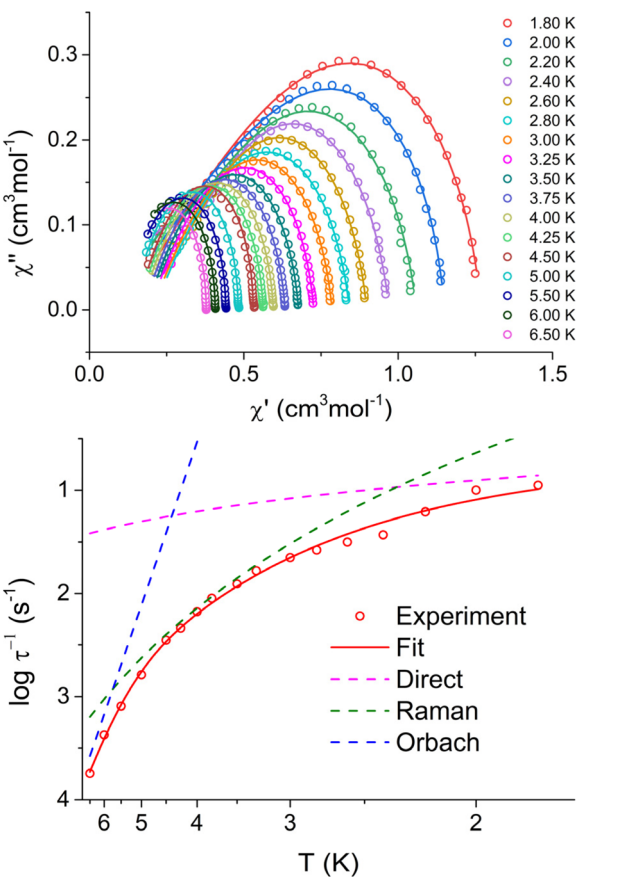

Fig. 3 Argand (Cole–Cole) diagram of in-phase and out-of-phase AC susceptibility (upper panel), and fit of relaxation time for **1** with eqn (6) and parameters listed in Table 4.

Table 4 Fitted parameters from analysis of relaxation processes

Complex	$\log \tau_0^{-1}$ (s^{-1})	U_{eff} (K)	C (s^{-1} K^{-5})	$\log A_{dir}$ (s^{-1} K^{-1} T^{-4})
1	8.45 ± 0.86	72.89 ± 12.59	0.14 ± 0.01	4.60 ± 0.05
2	6.26 ± 0.16	33.63 ± 1.64	0	4.58 ± 0.02
3	9.31 ± 0.17	50.53 ± 1.28	0	3.32 ± 0.03
5s[a]	0	0	0.15 ± 0.01	3.81 ± 0.07
5f	0	0	78.28 ± 12.24	5.89 ± 0.39

Complex	$\log \tau_0^{-1}$ (s^{-1})	U_{eff} (K)	$\log A_{dir}$ (s^{-1} K^{-1} T^{-4})	$\log B_1$ (s^{-1})	$\log B_2$ (s^{-1} T^{-2})
1Zn	5.79 ± 0.10	27.16 ± 0.75	3.52 ± 0.03	3.66 ± 0.06	6.11 ± 0.20

[a] As both processes were analyzed for **5**, they are marked as slower (s) and faster (f).

Consequently, we did not attempt to further analyze this minor process due to insufficient data. For complex **5**, two processes were observable throughout the entire temperature range, allowing us to analyze both of them. However, the data for the faster process was not of sufficient quality to provide a convincing analysis. Two options were tested for its analysis, the combination of Orbach + direct processes, and the combination of Raman + direct processes. The first choice (Raman + direct model) was chosen, because it provided reasonable values of fitted parameters, whereas the second option resulted in unrealistic small values of U_{eff}.

In the case of compounds **1**, **2**, and **3**, values of U_{eff} reasonably correlate with fitted D-parameters from the magnetic data. However, this correlation is not evident in the case of complex **5** for which we assume that the relaxation through the Raman process is too fast to observe Orbach relaxation.

To further study the relaxation of prepared compounds, complex **1** was selected as the most promising one and prepared again as a metal diluted sample with Zn(II), leading to complex **1Zn**. Magnetic measurements (in the range of temperatures 1.8–4.5 K for B = 0.1 T, and range of magnetic fields 0–0.5 T for T = 2 K) show quite a different relaxation profile from non-diluted **1**. We were able to fit the main relaxation process, but there seem to be other minor relaxation processes (some data seem to indicate even three relaxation channels) that we could not analyze in detail due to the insufficient resolution of these additional processes in **1Zn**. Therefore, we have focused only on fitting the most prominent process with clearly visible maxima. The following equation was used for fitting temperature and field-dependent data simultaneously:

$$\tau^{-1} = A_{dir} T H^{n_{dir}} + \frac{B_1}{1 + B_2 H^2} + \tau_0^{-1} e^{\frac{-U_{eff}}{T}} \quad (7)$$

The coefficient for direct relaxation was fixed (n_{dir} = 4) according to the literature as was done in eqn (6) for undiluted samples. However, the fitted U_{eff} for the diluted complex is significantly lower than U_{eff} of **1** (Table 4). The most striking difference between the relaxation in **1** and **1Zn** is the signature of zero-field relaxation observed in AC data suggested by the decrease of the in-phase and increase of the out-of-phase component of AC susceptibility close to the upper measurement frequency limit at 2 K. The relaxation time at zero static magnetic field of **1Zn** is 0.63 ms at 2 K, confirming thus that complex **1** can behave as zero-field SMM.

X-band EPR spectroscopy

The X-band EPR spectra of **1**, **1Zn**, **2**, **3**, **5**, and **6** were measured using powdered samples; the temperature evolution of the EPR spectra (Fig. S17†) shows a decrease of the signal intensity and a significant line broadening with increasing temperature with the lack of spectral details above 30 K. The spin-Hamiltonian and an effective S_{eff} = 1/2 Hamiltonian were used for the analysis of the experimental spectra obtained at 2.3 K. While spin Hamiltonian is often used to describe the two lowest Kramers doublets in Co(II), it is not possible to estimate the value of the D-parameter from X-band EPR for such large values as suggested from the analysis of magnetic data, only the sign of D and E/D ratio. On the other hand, for a large splitting between the ground and first excited Kramers doublet, highly anisotropic effective g-factors obtained from an effective S_{eff} = 1/2 Hamiltonian reflect the influence of higher electronic states and the anisotropy of the crystal field. The spectra were analyzed within the EasySpin Toolbox,[27] including hyperfine interaction (if resolved or necessary for the description) and an anisotropic convolutional broadening ΔB (full-width at half-height, which might reflect the unresolved hyperfine splitting). The splitting due to the hyperfine coupling parameter A was clearly identified only in the experimental EPR spectra of **1Zn** and **2** (see Fig. 4, S17, and S18†).

First, the analysis using spin Hamiltonian formalism was performed, clearly showing $D < 0$ for **2**, **3**, and **5** (see Fig. S17†). For the simulation, the D-parameter was tentatively set to ±10 cm^{-1}, and the obtained parameters are summarised in Table 5. Only one set of parameters was used to simulate the EPR spectra of **5**, but one cannot exclude the presence of a second Co(II) site with similar parameters. Regarding the analysis of **6**, the main component of the spectra at ~200 mT is clearly compatible with $D > 0$. The experiment did not resolve a possible contribution of the predicted Co(II) site with a negative D-parameter (*vide infra*); it might be due to the reduced signal intensity or different line broadening. Interestingly, the E/D ratio for **2**, **5**, and **6** well agrees with the analysis of magnetic data, while for **3** it seems closer to the CASSCF/NEVPT2

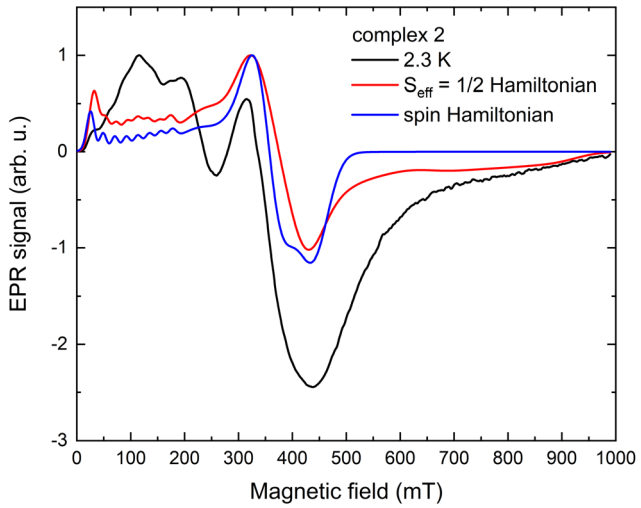

Fig. 4 X-band EPR spectra of **2** obtained at 2.3 K, including simulated spectra, an effective S_{eff} = 1/2 Hamiltonian and spin Hamiltonian models.

Table 5 Spin Hamiltonian parameters for compounds **2**, **3**, **5**, and **6** estimated from X-band EPR; only the sign of a large *D* parameter can be estimated

	D	*E*/*D*	g_x, g_y, g_z	ΔB_x, ΔB_y, ΔB_z (mT)	A_z (MHz)
2	−	0.295	2.12, 2.25, 2.35	50, 45, 55	700
3	−	0.056	2.15, 2.18, 2.38	40, 40, 180	
5	−	0.155	2.11, 2.16, 2.28	140, 130, 250	
6	+	0.180	2.40, 2.20, 2.00	70, 400, 120	

prediction. We could not reasonably reproduce the experimental EPR data of **1** and **1Zn** using the spin Hamiltonian approach, most probably due to a significant influence of hyperfine splitting; therefore, an effective S_{eff} = 1/2 Hamiltonian was used.

The results of the analysis of the EPR spectra using an effective S_{eff} = 1/2 Hamiltonian are summarised in Table 6. They can be understood in the frame of the model that includes spin–orbit coupling and a trigonal crystal field parameter δ to split the $^4T_1$ orbital triplet state originating from the cubic crystal field.[28] The obtained effective *g*-factors in the case of $\delta < 0$ equivalent to easy-axis anisotropy yield highly anisotropic $g'_z \gg g'_x, g'_y$ for $|\delta| > 1000$ cm^{-1}, similar to the ones obtained for **1**, **1Zn**, **2**, **3**, and **5**. Unlike our previous studies, the two lower *g*-factor components do not reach the theoretical

Table 6 Effective S_{eff} = 1/2 Hamiltonian parameters for compounds **1**, **1Zn**, **2**, **3**, **5**, and **6** estimated from X-band EPR

	g'_x, g'_y, g'_z	A'_x, A'_y, A'_z (MHz)	ΔB_1, ΔB_2, ΔB_3 (mT)
1	0.68, 2.40, 7.17	110, 580, 650	50, 45, 55
1Zn	0.71, 2.50, 7.17	110, 720, 630	20, 22, 22
2	0.83, 1.77, 6.45	350, 290, 1800	40, 55, 65
3	0.82, 1.79, 6.15	400, 300, 650	20, 80, 100
5	0.74, 1.00, 6.10		120, 160, 180
6	—, 3.39, —		

predictions of the quasi-degenerate perturbation theory.[29] In the case of **6**, a strong central resonance line was assigned to g' = 3.39 characteristic for $\delta > 0$ (easy-plane anisotropy). Interestingly, for **1** and **1Zn**, slightly different *g*-factors and hyperfine interaction parameters were needed to simulate the two datasets (Fig. S17†). The full hyperfine splitting pattern was not resolved even in the diluted sample. Differences in obtained parameters might suggest that the Co(II) dilution also leads to minor changes in its electronic spectra.

Theoretical calculations

Theoretical CASSCF/NEVPT calculations were conducted to provide additional insights into the electronic structure of the prepared complexes and to potentially identify structural correlations and elucidate the magnetic behavior of the studied compounds. The calculations were performed using molecular structures derived from the X-ray data, and only the atomic positions of the hydrogen atoms were optimized using the DFT method.

The energy levels and zero-field splitting (ZFS) parameters of the studied complexes were calculated using the complete active space self-consistent field method (CASSCF) with a 7-electron in 5-orbital active space (CAS(7,5)), which corresponds to the Co(II) $3d^7$ electron configuration. The treatment of dynamic electron correlation was performed using the N-electron valence perturbation theory (NEVPT2) method. The energy of the active metal d-orbitals was calculated using the AILFT (*Ab Initio* Ligand Field Theory) module in ORCA.

In the case of an ideal trigonal prismatic geometry, the d-orbitals are split into three energy levels. The lowest level corresponds to the d_{z^2} orbital, followed by two degenerate orbitals, d_{xy} and $d_{x^2-y^2}$, and the highest level consists of two degenerate orbitals, d_{xz} and d_{yz}. Such ordering of orbitals is clearly visible for all complexes except for **3** and **6b**, suggesting that most of the prepared complexes have crystal field splitting similar to the trigonal prism (Fig. 5).

In a free Co(II) ion, its ground atomic term is ^4F, which is then followed by two excited states ^4P and ^2G. In ideal O_h symmetry, ^4F is split into $^4T_1$ + $^4T_2$ + $^4A_1$ ligand field terms, ^4P into the $^4T_1$ ligand field term, and ^2G into $^2T_1$ + $^2T_2$ + $^2A_1$ ligand field terms. If symmetry is reduced further to D_3, each ^4T term splits into ^4E and ^4A, therefore ground term ^4F is split into ^4E + ^4E + $^4A_2$ + $^4A_1$ $^4A_2$, as is observed in the trigonal prism Tanabe Sugano diagram.[30] After further reduction of symmetry by distortion from the ideal shape, ^4E terms are split into 2 levels. Therefore, the ^4F term splits into 7 non-degenerate levels (ligand field terms) in non-ideal symmetry. Thus, if the coordination polyhedron is close to the trigonal prism shape, it should be theoretically possible to see distribution similar to original terms – two close-lying levels from the ground ^4E term, another two levels from the first excited ^4E term, and finally three levels from ^4A terms. It is possible to spot this energy level distribution on prepared complexes, mainly **1** and **4** (Fig. 5). Above ground term levels, 3 quartet levels are visible, which are originating in ^4E and $^4A_2$ from ^4P first excited term,

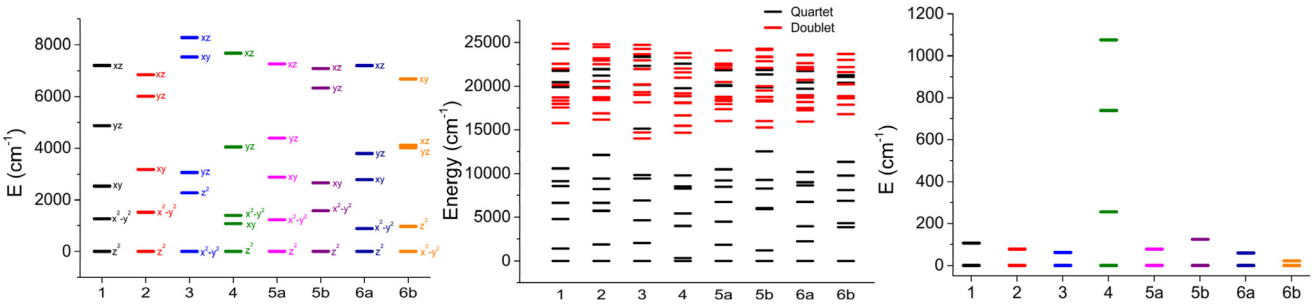

Fig. 5 *Ab initio* energy of d-orbitals (left panel), ligand field terms (center panel), and ligand field multiplets (right panel) for studied complexes.

and also a large number of doublet states, which are from ^{2}G and also higher doublet terms.

The spin–orbit interaction further splits the $^4\Gamma$ ground term into two ligand field multiplets. Theoretically, the D_{3h} symmetry is expected to yield large and negative *D*-parameters. Our calculations have confirmed this assumption, and all the relevant parameters for the studied compounds are listed in Table 7 and Table S8†

Based on the results, it can be observed that among the studied complexes, **5b** and **1** exhibit the most favorable characteristics due to their large negative *D*-parameter. However, it is worth noting that this is a common feature among almost all the complexes, except for the unusual case of **6b**, which appears to have an easy-plane anisotropy with its positive *D*-parameter and significant rhombic components of the *g*-tensor. The ZFS and *g*-factor parameters for complex **4** are approximate because its low-lying excited states (Fig. 5) exclude the application of spin Hamiltonian formalism. Additionally, this is often associated with a larger anisotropy, as evidenced by the significant splitting of the crystal field multiplets (Fig. 5).

Moreover, we analyzed the variation of the calculated *D*-parameter within the series for complexes with a geometry close to the trigonal prism, namely, we took into account complexes **1**, **2**, **4**, **5a**, **5b**, and **6a** that all have the splitting of d-orbitals resembling the expected one for non-ideal D_{3h} symmetry. In such a case, the largest contribution to the *D*-parameter stems from the electron excitation from ground state electronic configuration $d_{z^2}^2 d_{x^2-y^2}^2 d_{xy}^1 d_{yz}^1 d_{xz}^1$ to the first excited state electronic configuration $d_{z^2}^2 d_{x^2-y^2}^1 d_{xy}^2 d_{yz}^1 d_{xz}^1$, which corresponds to the electron transfer between $d_{x^2-y^2}$ and d_{xy} orbitals. Note that in the case of complex **4**, the ordering of these two orbitals is interchanged. Anyway, these two orbitals have the same $|m_l|$ values and thus such excitation ($d_{x^2-y^2} \leftrightarrow d_{xy}$) has a large contribution to the D_{zz} part of the *D*-tensor, which induces a large negative value of the *D*-parameter.[31] The slight energy difference between these orbitals in **4** results in a configuration that closely resembles the orbitally degenerate ^{4}E′ ground state term. Thus, it is not surprising that calculated anisotropy is huge and axial, with limited validity of spin Hamiltonian formalism (Table 7).

Indeed, the respective correlation was established between the *D*-parameter and the energy difference of two d-orbitals $\Delta\varepsilon_d = |\varepsilon(d_{xy}) - \varepsilon(d_{x^2-y^2})|$ as depicted in Fig. 6. Evidently, the magnetic anisotropy parameters are very sensitive to the changes in the shape of the coordination polyhedron reflected in d-orbitals splitting induced by the respective ligand field.

Table 7 Calculated spin Hamiltonian parameters and *g*-factors for studied complexes

	D (cm^{-1})	E/D	g_x	g_y	g_z	Δ^b (cm^{-1})
1	−52.54	0.074	2.216	2.096	2.760	−103.41
2	−38.40	0.050	2.128	2.188	2.602	−77.07
3	−30.70	0.054	2.153	2.177	2.505	−61.67
4[a]	*−127.73*	*0.022*	*1.849*	*2.000*	*3.377*	−255.66
5a	−37.62	0.129	2.113	2.250	2.623	−77.1
5b	−61.87	0.014	2.099	2.147	2.823	−123.78
6a	−27.43	0.232	2.120	2.294	2.532	−59.13
6b	10.83	0.075	2.159	2.290	2.305	21.83

[a] For **4**, spin Hamiltonian parameters are not completely relevant, because it is not possible to fully describe its energy level splitting with spin Hamiltonian formalism. [b] The parameter Δ is defined as the energy difference of the two lowest Kramers doublets.

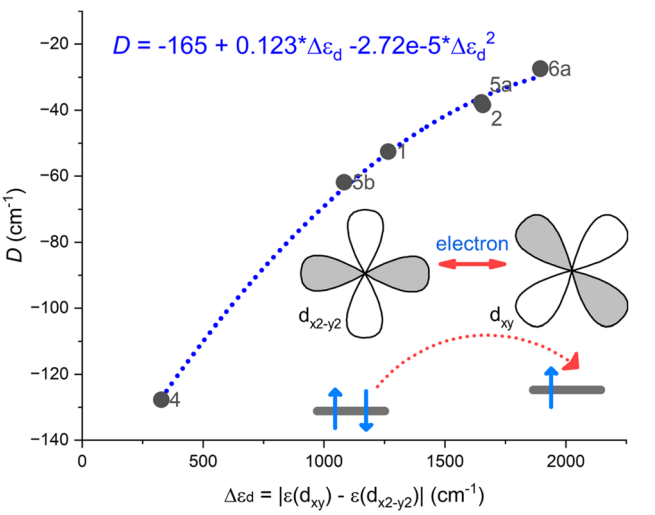

Fig. 6 A correlation established between the *D*-parameter and the energy difference of two d-orbitals $\Delta\varepsilon_d = |\varepsilon(d_{xy}) - \varepsilon(d_{x^2-y^2})|$ using CASSCF/NEVPT2 results for complexes **1**, **2**, **4**, **5a**, **5b**, and **6a**.

To gain a deeper understanding of magnetic behavior, we utilized the computational module SINGLE_ANISO, which enabled us to visualize the anisotropic energy barrier and calculate transition rates as magnetic moment matrix elements. These transition rates provide valuable insights into the probability of relaxation processes and help identify the pathways for magnetization reversal transitions. In the case of a Co(II) system with a spin of 3/2, there are only two Kramers doublets that could potentially be involved in the relaxation. Of particular importance is the transition rate associated with the ground state quantum tunneling of magnetization, as it determines whether the higher Kramers doublet will play a major role in the relaxation mechanism. The output of the SINGLE_ANISO module is depicted in Fig. 7 for **2**, and in Fig. S19† for the rest of the complexes.

Thus, it is evident that complexes **4** and **5b** exhibit the smallest tunneling probabilities in their ground state, which aligns with previous findings describing these complexes as highly anisotropic. These complexes demonstrate tunneling probabilities below 0.1, which render them potential zero-field SMMs. On the other hand, complexes **1**, **2**, and **3** exhibit tunneling probabilities above 0.1, suggesting that quantum tunneling of magnetization (QTM) is likely to play a significant role in their relaxation. However, it is possible to suppress QTM by applying a magnetic field, which transforms these compounds into field-induced single-molecule magnets (SMMs). Finally, complexes **5a** and **6a** show a high probability of QTM, while complex **6b** is predicted to have typical easy-plane spin level splitting, indicating no potential for slow relaxation of magnetization.

To assess the preference of ligand scaffold in complexes **1–6** for trigonal geometry, we chose to perform additional DFT optimizations on their molecular structures in a vacuum with the help of the well-established B3LYP functional. This approach allows us to explore their optimal arrangement while excluding the influence of crystal packing effects. Indeed, the coordination polyhedra in the optimized geometries of all the complexes exhibit a tendency to adopt trigonal symmetry, characterized by relatively modest TP CSM values ranging between 1.6 and 3.7, and τ_6 values found between 0.62 and 0.86 (Table S9†). Remarkably, this inclination persists despite the substantial relaxation observed in the calculated molecular geometries. Evidently, this relaxation is reflected in the elongation of metal–ligand bond lengths, particularly those with the etheric oxygen atoms (O2 and O3), which extend well beyond 2.35 Å (Table S9†). Thus, it seems that the herein utilized ligand motif is rigid enough to provide Co^{II} complexes with a ligand field close to D_3 symmetry and certainly deserves further exploration.

We opted to compare our findings also with the data available in CSD. Our search yielded eight crystal structures of complexes containing the Co, Ni and Zn metal centers coordinated with the 2-formylphenoxyacetic acid based Schiff base ligands. Notably, all these complexes incorporate either identical or their methoxy derivatives as those used in the synthesis of **1** and **3**. Specifically, these ligands feature either ethylene (en) or propylene (pr) linkers in their structures.

Upon examining their coordination polyhedra, we observed that these complexes primarily adopt coordination environments that closely resemble either octahedral (Oh) or trigonal prismatic (TP) geometries – Table S10.† Complexes with en linkers tend to favor a trigonal prismatic coordination. Even when the lowest CSM values indicate an octahedral geometry, these values are notably high (>5; CSD codes: RUJNES,[20] SIRMOX[32]), comparable to those calculated for a TP geometry. This suggests significant distortion from an idealized octahedral shape.

Conversely, complexes featuring pr linkers and adopting an Oh geometry (CSD codes: HOMFOF,[17] QEBBIL,[19] SIRMUD[32]) exhibit low CSM values (below 1.56), implying minimal deviation from an ideal octahedral shape. Given that a TP geometry would induce a doubly degenerate ground state for the Co(II) central atom—subject to strong Jahn–Teller distortion—it is reasonable to conclude that ligand rigidity, particularly in ligands with shorter en linkers, plays a key role in stabilizing this geometry.[33]

These observations are consistent with the crystal structures presented in this study. The most significant deviation from a TP geometry was observed in **3** featuring a pr linker (Table 2; CSM TP = 4.727, CSM Oh = 5.626). Interestingly, complex **4** featuring a 2-hydroxypropyl linker closely approximated an ideal TP geometry, even though its linker length is very similar to that of the pr linker. However, this complex also incorporates a hydroxyl group, which influences the overall structure not only through steric hindrance but also by enabling intermolecular hydrogen bonding.

These findings lead to a consideration of the somewhat unpredictable effects of crystal packing and non-covalent interactions. For example, the cobalt coordination environments in solvatomorph **3** and HOMFOF differ markedly. Solvatomorph **3** is a methanol solvate, while HOMFOF contains six co-crystallized water molecules per complex in its structure. Notably,

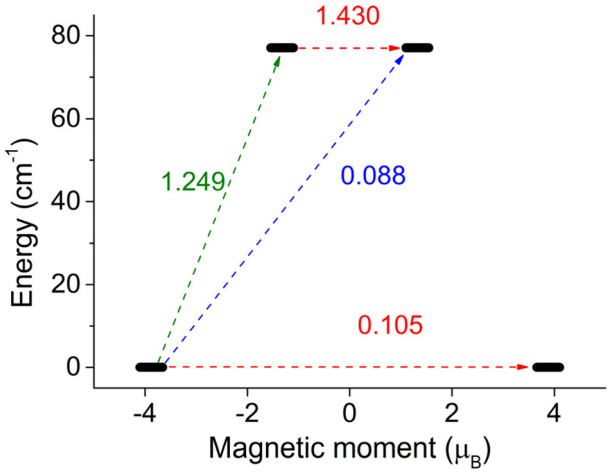

Fig. 7 SINGLE_ANISO description of the magnetic moment matrix elements between Kramers doublets for complex **2**.

complexes approximating an Oh geometry frequently feature extensive solvation in their second coordination spheres, as evidenced by the examples of HOMFOF, SIRMOX, and SIRMUD.

In summary, we may conclude that DFT calculations can predict the geometry of these complexes with reasonable accuracy – Fig. S20.† A general guideline could be that rigid linkers in Schiff base ligands based on 2-formylphenoxyacetic acid contribute to the stabilization of a TP geometry in Co(II) complexes. However, this conclusion must be interpreted with caution, as non-covalent interactions, and particularly the co-crystallization of solvent molecules, can significantly influence the geometry of complex molecules in the solid state.

Experimental

General methods

(2-Formylphenoxy)acetic acid was prepared by a previously published method.[34] All the complexes were prepared by *in situ* reactions of (2-formylphenoxy)acetic acid, respective amine, and cobalt(II) acetate. The reagents were purchased from commercial sources. The CHNS elementary analysis was done using a Thermo Scientific Flash 2000 analyzer (Thermo Scientific, Waltham, MA, USA). The IR spectra were recorded using a Jasco FT/IR-4700 spectrometer (Jasco, Easton, MD, USA) using the ATR technique on a diamond plate in the spectral range of 400–4000 cm^{-1}. The powder XRD patterns were measured using a Rigaku MiniFlex600 diffractometer (Rigaku, Austin, TX, USA) equipped with the Bragg–Brentano geometry and using Cu Kα radiation. EPR spectra were measured on powdered samples using a Bruker ELEXSYS II E500 spectrometer.

Synthesis

[Co(fpa-en)]·MeOH (1). In 10 ml of methanol, 72 mg of (2-formylphenoxy)acetic acid (0.4 mmol) was mixed with 50 mg of $Co(CH_3COO)_2{\cdot}4H_2O$ (0.2 mmol). The mixture was stirred for 10 minutes, then 12 mg of 1,2-ethylenediamine (0.2 mmol) was added. The mixture was then refluxed for an hour, during which it changed color to wine red or purple. The mixture was then left to stand for three days, which produced needle-like crystals, which were filtered off and washed with diethylether. Crystals suitable for X-ray diffraction were grown by diffusion of diethyl ether vapors into solution.

Anal. calcd for $C_{21}H_{22}N_2O_7Co$ (**1**): M_{mol} = 473.35 g mol^{-1} – C 53.29; H 4.68; N 5.92%. Found: C 53.08; H 5.08; N 5.88%.

FTIR (ATR, cm^{-1}): 3262 (m), 3053 (w), 2940 (w), 1620 (s), 1494 (s), 1383 (s), 1341 (s), 1244 (s), 1132 (m), 1015 (s), 940 (m), 891 (m), 753 (s), 598 (w), 528 (w).

[Co(fpa-pda)]·DMSO (2). In 10 ml of methanol, 72 mg of (2-formylphenoxy)acetic acid (0.4 mmol) was mixed with 50 mg of $Co(CH_3COO)_2{\cdot}4H_2O$ (0.2 mmol). The mixture was stirred for 10 minutes, then 21.6 mg of *o*-phenylenediamine (0.2 mmol) was added and the mixture was refluxed for an hour, which resulted in the precipitation of red powder. This powder was filtered off, washed with methanol and diethylether and dried. After this, the powder was recrystallized from a mixture of methanol and dimethylsulfoxide (DMSO was added dropwise to the suspension of the powder in methanol until it fully dissolved) by diffusion of diethyl ether vapors, which resulted in red crystals, which were filtered and washed with diethylether.

Anal. calcd for $C_{26}H_{24}N_2O_7SCo$ (**2**): M_{mol} = 567.48 g mol^{-1} – C 55.03; H 3.91; N 4.94; S 5.65%. Found: C 54.51; H 4.15; N 4.94; S 5.07%.

FTIR (ATR, cm^{-1}): 3033 (w), 2991 (w), 2911 (s), 2165 (w), 1981 (w), 1638 (s), 1485 (s), 1380 (s), 1282 (s), 1237 (s), 1161 (m), 939 (m), 822 (m), 751 (s), 614 (w), 518 (w).

[Co(fpa-pn)]·MeOH (3). In 5 ml of propanol and 1 ml of methanol, 72 mg of (2-formylphenoxy)acetic acid (0.4 mmol) was mixed with 50 mg of $Co(CH_3COO)_2{\cdot}4H_2O$ (0.2 mmol). The mixture was stirred for 10 minutes, then 15 mg of 1,3-propylenediamine (0.2 mmol) was added, and the mixture was gently heated for 20 minutes. Then, the product was crystallized by diffusion of diethyl ether vapors, which resulted in purple plate-like crystals, which were filtered off and washed with diethyl ether.

Anal. calcd for $C_{22}H_{24}N_2O_7Co$(**3**): M_{mol} = 487.38 g mol^{-1} – C 54.22; H 4.55; N 5.75%. Found: C 53.45; H 4.87; N 5.70%.

FTIR (ATR, cm^{-1}): 3725 (w), 3630 (w) 3276 (m), 3080(w), 2930 (m), 2820 (w), 2297 (w), 2165 (w), 1618 (s), 1493 (s), 1437 (s), 1247 (m), 1128 (m), 1018 (s), 937 (m), 887 (m), 817 (m), 759 (s), 708 (m), 521 (w), 454 (w), 362 (w).

[Co(fpa-OHpn)]·MeOH (4). In 10 ml methanol, 72 mg of (2-formylphenoxy)acetic acid (0.4 mmol) was mixed with 50 mg of $Co(CH_3COO)_2{\cdot}4H_2O$ (0.2 mmol). The mixture was stirred and slightly heated for 5 minutes, and then 18 mg of 2-hydroxy-1,3-propylenediamine (0.2 mmol) was added; after another 5 minutes, a purple solution was obtained and left to crystallize by diffusion of diethyl ether, which produced a small amount of purple crystals.

[Co(fpa-cn)]·MeOH (5). In 5 ml of propanol and 1 ml of methanol, 72 mg of (2-formylphenoxy)acetic acid (0.4 mmol) was mixed with 50 mg of $Co(CH_3COO)_2{\cdot}4H_2O$ (0.2 mmol). The mixture was stirred for 10 minutes, then 23 mg of cyclohexane-1,2-diamine (0.2 mmol) was added, and the mixture was gently heated for 20 minutes. Then, the product was crystallized by diffusion of diethyl ether vapors, which resulted in purple crystals, which were filtered off and washed with diethyl ether.

Anal. calcd for $C_{25}H_{28}N_2O_7Co$(**5**): M_{mol} = 527.44 g mol^{-1} – C 56.93; H 4.97; N 5.31%. Found: C 56.57; H 4.79; N 5.11%.

FTIR (ATR, cm^{-1}): 3411 (w), 3062 (w), 2929 (m), 2859 (m), 2166 (w), 1628 (s), 1497 (s), 1449 (s), 1381 (s), 1286 (s), 1128 (m), 1004 (s), 939 (m), 894 (m), 821 (m), 759 (s), 614 (w), 515 (w), 453 (w), 400 (w), 353 (w).

[Co(fpa-dpen)] (6). In 5 ml of propanol and 1 ml of methanol, 72 mg of (2-formylphenoxy)acetic acid (0.4 mmol) was mixed with 50 mg of $Co(CH_3COO)_2{\cdot}4H_2O$ (0.2 mmol). The mixture was stirred for 10 minutes, then 42 mg of 1,2-diphenylethylen-1,2-diamine (0.2 mmol) was added, and the mixture was gently heated for 20 minutes. Then, the product

was crystallized by diffusion of diethyl ether vapors, which resulted in purple crystals, which were filtered off and washed with diethyl ether.

Anal. calcd for $C_{32}H_{26}N_2O_7Co$(**6**): M_{mol} = 593.51 g mol^{-1} – C 64.76; H 4.08; N 4.72%. Found: C 64.23; H 4.41; N 4.53%.

FTIR (ATR, cm^{-1}): 3724 (m), 3598 (w), 3398 (m), 3031 (w), 2913 (w), 2360 (w), 2298 (w), 2113 (w), 1982 (w), 1619 (s), 1492 (s), 1376 (s), 1293 (s), 1131 (s), 1027 (s), 937 (m), 827 (m), 754 (s), 702 (s), 596 (m), 519 (w), 458 (w).

[$Co_{0.026}Zn_{0.973}$(fpa-en)]·MeOH (1Zn). In 10 ml of methanol, 72 mg of (2-formylphenoxy)acetic acid (0.4 mmol) was mixed with 5 mg of $Co(CH_3COO)_2·4H_2O$ (0.02 mmol) and 39 mg of $Zn(CH_3COO)_2·2H_2O$ (0.18 mmol). The mixture was stirred for 10 minutes, then 12 mg of 1,2-ethylenediamine (0.2 mmol) was added. The mixture was then refluxed for an hour, during which it changed color to light purple. The mixture was then left to stand for three days, which produced crystals, which were filtered off and washed with diethylether.

Anal. calcd for $C_{21}H_{22}N_2O_7Co_{0.027}Zn_{0.974}$ (**1Zn**): M_{mol} = 479.66 g mol^{-1} – C 52.59; H 4.20; N 5.84%. Found: C 52.35; H 4.49; N 5.72%.

Theoretical calculations

All theoretical calculations were performed with the use of the ORCA 5.0.2. program package.[35] Initial molecular structures, obtained from X-ray data were treated by DFT hydrogen optimization, with the BP86 functional,[36] with basis sets from Ahlrich def2 basis set,[37] QZVP basis for Co, SVP for C and H atoms, and TZVP for other atoms, and def2/J auxiliary basis. Fully optimized molecular structures reported in Table S9† were obtained with the B3LYP[38] hybrid DFT functional with the help of D4 dispersion correction,[39] and the vibrational analyses confirmed proper convergence for complexes at local energy minimum as there were no imaginary frequencies.

CASSCF calculations were done with the TZVPP basis for Co and the TZVP basis for all other atoms and with def2/J and def2-TZVP/C auxiliary basis sets. The dynamic electron correlation was treated by the RI-NEVPT2 method,[40] and spin–orbit coupling by RI-SOMF(1×) approach.[41] CASSCF was performed for 7 electrons in 5 d-orbitals (selected by ORCA keyword "actorbs dorbs"), which corresponds to the Co(II) valence electron configuration. The number of calculated roots responds to a maximal number of possible roots, 10 states with multiplicity M_S = 4 and 40 roots with M_S = 2. For further analysis of Kramers doublets, the SINGLE_ANISO module[42] was used and set up to calculate with two Kramers doublets. CASSCF calculations were done with the "NoFrozenCore" keyword.

All calculations were performed with the help of the RIJCOSX approximation,[43] with improved integral precision, enabled by "DEFGRID3" ORCA keyword, and strict convergence "TightSCF" settings.

For visualization, the software Avogadro[44] and Mercury[45] were used. Magnetic data were analyzed with the help of software PHI[46] and RELACS.[47] In some parts of the text, ChatGPT 3[48] was used for grammar and stylistic corrections.

Conclusions

A series of six novel complexes were synthesized and characterized using a combination of theoretical and experimental methods, focusing on magnetic properties. These complexes exhibit a notable inclination towards adopting a trigonal prismatic geometry, as confirmed by both experimental observations and theoretical DFT calculations. This inclination is influenced by the building blocks employed in constructing the Schiff base ligand. This observation suggests the potential for further adjustments and fine-tuning of the system to enhance its performance in potential applications. Overall, this system demonstrates remarkable versatility and holds substantial promise for further molecular optimization.

The magnetic properties of the studied complexes were investigated using DC and AC magnetometry, as well as EPR spectroscopy. The obtained results were used to extract the parameters of the spin Hamiltonian. Four of the studied complexes were experimentally confirmed to have large and negative *D*-parameter, indicating axial anisotropy, while complex **6** showed a positive *D*-parameter. These experimental findings were also supported by theoretical calculations.

AC magnetic measurements revealed that the prepared complexes exhibit characteristics of field-induced single-molecule magnets, as evidenced by the significant quantum tunneling of magnetization in the ground state even without the presence of a magnetic field. In the presence of a magnetic field, all of the prepared complexes demonstrate a slow relaxation of magnetization, including also complex **6** which exhibits easy-plane magnetic anisotropy. The observed field induced magnetic relaxation of **6** can be attributed either to the Raman relaxation process or to the presence of complex **6a** within the asymmetric unit which possesses the axial type magnetic anisotropy suitable for the Orbach relaxation process as suggested by theoretical calculations.

The most interesting results were obtained for zinc-diluted sample **1Zn**, for which the slow relaxation of magnetization was observed already at zero static magnetic field. Interestingly, the dilution of the sample resulted in changes in spin Hamiltonian parameters as evidenced by EPR analysis and also in changes in the parameters describing the magnetization relaxation processes. Nevertheless, these results make the utilized ligand scaffold promising for future preparation of zero-field SMMs.

Conflicts of interest

There are no conflicts to declare.

Acknowledgements

We acknowledge financial support from the Palacký University Olomouc project IGA_PrF_2022_006. E. Č. was supported by the Slovak Research and Development Agency, contract no.

APVV-22-0172 and APVV-18-0197. We also thank Mrs. Pavla Richterová for performing elemental analysis.

References

1 A. Caneschi, D. Gatteschi, R. Sessoli, A. L. Barra, L. C. Brunel and M. Guillot, Alternating Current Susceptibility, High Field Magnetization, and Millimeter Band EPR Evidence for a Ground S = 10 State in $[Mn_{12}O_{12}(CH_3COO)_{16}(H_2O)_4]\cdot 2CH_3COOH\cdot 4H_2O$, *J. Am. Chem. Soc.*, 1991, **113**(15), 5873–5874, DOI: **10.1021/ja00015a057**.

2 M. Feng and M. L. Tong, Single Ion Magnets from 3d to 5f: Developments and Strategies, *Chem. – Eur. J.*, 2018, **24**(30), 7574–7594, DOI: **10.1002/chem.201705761**.

3 F. A. Cotton, *Progress in Inorganic Chemistry (Vol.6)*, Interscience Publishers, 1964.

4 A. Sarkar, S. Dey and G. Rajaraman, Role of Coordination Number and Geometry in Controlling the Magnetic Anisotropy in Fe^{II}, Co^{II}, and Ni^{II} Single–Ion Magnets, *Chem. – Eur. J.*, 2020, **26**(62), 14036–14058, DOI: **10.1002/chem.202003211**.

5 (*a*) R. Herchel, L. Váhovská, I. Potočňák and Z. Trávníček, Slow Magnetic Relaxation in Octahedral Cobalt(II) Field-Induced Single-Ion Magnet with Positive Axial and Large Rhombic Anisotropy, *Inorg. Chem.*, 2014, **53**(12), 5896–5898, DOI: **10.1021/IC500916U**; (*b*) I. Nemec, R. Herchel, M. Kern, P. Neugebauer, J. van Slageren and Z. Trávníček, Magnetic Anisotropy and Field–Induced Slow Relaxation of Magnetization in Tetracoordinate Co^{II} Compound $[Co(CH_3{-}im)_2Cl_2]$, *Materials*, 2017, **10**(3), 249, DOI: **10.3390/MA10030249**.

6 G. A. Craig and M. Murrie, 3d Single-Ion Magnets, *Chem. Soc. Rev.*, 2015, **44**(8), 2135–2147, DOI: **10.1039/C4CS00439F**.

7 (*a*) S. Alvarez, Polyhedra in (Inorganic) Chemistry, *Dalton Trans.*, 2005, (13), 2209, DOI: **10.1039/b503582c**; (*b*) S. Alvarez, P. Alemany, D. Casanova, J. Cirera, M. Llunell and D. Avnir, Shape Maps and Polyhedral Interconversion Paths in Transition Metal Chemistry, *Coord. Chem. Rev.*, 2005, **249**(17–18 SPEC. ISS.), 1693–1708, DOI: **10.1016/j.ccr.2005.03.031**; (*c*) D. Casanova, P. Alemany, J. M. Bofill and S. Alvarez, Shape and Symmetry of Heptacoordinate Transition-Metal Complexes: Structural Trends, *Chem. – Eur. J.*, 2003, **9**(6), 1281–1295, DOI: **10.1002/chem.200390145**; (*d*) A. Ruiz-Martínez, D. Casanova and S. Alvarez, Polyhedral Structures with an Odd Number of Vertices: Nine-Atom Clusters and Supramolecular Architectures, *J. Chem. Soc., Dalton Trans.*, 2008, (19), 2583–2591, DOI: **10.1039/b718821h**.

8 B. Yao, M. K. Singh, Y.-F. Deng, Y.-N. Wang, K. R. Dunbar and Y.-Z. Zhang, Trigonal Prismatic Cobalt(II) Single-Ion Magnets: Manipulating the Magnetic Relaxation Through Symmetry Control, *Inorg. Chem.*, 2020, **59**(12), 8505–8513, DOI: **10.1021/acs.inorgchem.0c00950**.

9 V. V. Novikov, A. A. Pavlov, Y. V. Nelyubina, M.-E. Boulon, O. A. Varzatskii, Y. Z. Voloshin and R. E. P. Winpenny, A Trigonal Prismatic Mononuclear Cobalt(II) Complex Showing Single-Molecule Magnet Behavior, *J. Am. Chem. Soc.*, 2015, **137**(31), 9792–9795, DOI: **10.1021/jacs.5b05739**.

10 A. A. Pavlov, D. Y. Aleshin, S. A. Savkina, A. S. Belov, N. N. Efimov, J. Nehrkorn, M. Ozerov, Y. Z. Voloshin, Y. V. Nelyubina and V. V. Novikov, A Trigonal Prismatic Cobalt (II) Complex as a Single Molecule Magnet with a Reduced Contribution from Quantum Tunneling, *ChemPhysChem*, 2019, **20**(8), 1001–1005, DOI: **10.1002/cphc.201900219**.

11 A. A. Pavlov, S. A. Savkina, A. S. Belov, Y. V. Nelyubina, N. N. Efimov, Y. Z. Voloshin and V. V. Novikov, Trigonal Prismatic Tris-Pyridineoximate Transition Metal Complexes: A Cobalt(II) Compound with High Magnetic Anisotropy, *Inorg. Chem.*, 2017, **56**(12), 6943–6951, DOI: **10.1021/acs.inorgchem.7b00447**.

12 T. J. Ozumerzifon, I. Bhowmick, W. C. Spaller, A. K. Rappé and M. P. Shores, Toward Steric Control of Guest Binding Modality: A Cationic Co(II) Complex Exhibiting Cation Binding and Zero-Field Relaxation, *Chem. Commun.*, 2017, **53**(30), 4211–4214, DOI: **10.1039/C7CC01172E**.

13 B. Yao, Y.-F. Deng, T. Li, J. Xiong, B.-W. Wang, Z. Zheng and Y.-Z. Zhang, Construction and Magnetic Study of a Trigonal-Prismatic Cobalt(II) Single-Ion Magnet, *Inorg. Chem.*, 2018, **57**(22), 14047–14051, DOI: **10.1021/acs.inorgchem.8b02692**.

14 Y. Y. Zhu, Y. Q. Zhang, T. T. Yin, C. Gao, B. W. Wang and S. Gao, A Family of $Co^{II}Co^{III}_3$ Single-Ion Magnets with Zero-Field Slow Magnetic Relaxation: Fine Tuning of Energy Barrier by Remote Substituent and Counter Cation, *Inorg. Chem.*, 2015, **54**(11), 5475–5486, DOI: **10.1021/ACS.INORGCHEM.5B00526**.

15 I. Nemec, O. F. Fellner, B. Indruchová and R. Herchel, Trigonally Distorted Hexacoordinate Co(II) Single-Ion Magnets, *Materials*, 2022, **15**(3), 1064, DOI: **10.3390/ma15031064**.

16 J. Wang, D.-S. Zhu, K.-Z. Shao and L. Xu, {2,2′-[Ethane-1,2-Diylbis(Nitrilomethylidyne)]Diphenoxyacetato}zinc(II) Methanol Solvate, *Acta Crystallogr., Sect. E: Struct. Rep. Online*, 2006, **62**(8), m1884–m1886, DOI: **10.1107/S1600536806026791**.

17 Z. L. Wang, D. S. Zhu and R. S. Wang, Crystal Structure of [N,N′-(Bis(2-Phenoxyacetic)Formylidene)Propane- 1,3-Diaminecobalt(II)] Hexahydrate, $[Co(C_{21}H_{20}N_2O_6)]\cdot 6H_2O$, *Z. Kristallogr. – New Cryst. Struct.*, 2008, **223**(3), 217–218, DOI: **10.1524/NCRS.2008.0091**.

18 Z. L. Wang, D. S. Zhu and R. S. Wang, Crystal Structure of [N,N′-(Bis(2-Phenoxyacetic)Formylidene)Propane- 1,3-Diamine-Zinc(II)] - Water - Ethanol (1 : 1 : 0.25), $[Zn(C_{21}H_{20}N_2O_6)]\cdot H_2O\cdot 0.25C_2H_6O$, *Z. Kristallogr. – New Cryst. Struct.*, 2008, **223**(3), 215–216, DOI: **10.1524/NCRS.2008.0090/DOWNLOADASSET/1267-2227.CFF**.

19 L. Yan and C. L. Liu, Synthesis, Structure Characterization, Antibacterial Activity and Fluorescence Studies of a Ni(II) Compound with Schiff-Base Ligand, *Jiegou Huaxue*, 2017, **36**(8), 1315–1320, DOI: **10.14102/J.CNKI.0254-5861.2011-1522**.

20 L. Yan, W. Liu, M. J. Wang, Y. Xu and K. Z. Shi, Synthesis, Characterization, Oxygen Respiratory, Antibacterial Activity, and Photoluminescent Property Studies of One Novel Complex with Schiff-Base Ligand, *Jiegou Huaxue*, 2020, **39**(5), 895–900, DOI: 10.14102/J.CNKI.0254-5861.2011-2585.

21 P. van der Sluis and A. L. Spek, BYPASS: An Effective Method for the Refinement of Crystal Structures Containing Disordered Solvent Regions, *Acta Crystallogr., Sect. A: Found. Crystallogr.*, 1990, **46**(3), 194–201, DOI: 10.1107/S0108767389011189.

22 J. Moncol, Geometry index for 6-coordinate compounds, *Czech Chem. Soc. Symp. Ser.*, 2023, **21**, 147.

23 (*a*) A. W. Addison, T. N. Rao, J. Reedijk, J. van Rijn and G. C. Verschoor, Synthesis, Structure, and Spectroscopic Properties of Copper(II) Compounds Containing Nitrogen–sulphur Donor Ligands; the Crystal and Molecular Structure of Aqua[1,7-Bis(N-Methylbenzimidazol-2′-Yl)-2,6-Dithiaheptane] Copper(II) Perchlorate, *J. Chem. Soc., Dalton Trans.*, 1984, 1349–1356, DOI: 10.1039/DT9840001349; (*b*) L. Yang, D. R. Powell and R. P. Houser, Structural Variation in Copper (I) Complexes with Pyridylmethylamide Ligands: Structural Analysis with a New Four-Coordinate Geometry Index, τ_4, *Dalton Trans.*, 2007, 955–964, DOI: 10.1039/B617136B.

24 O. Kahn, *Molecular magnetism*, VCH, 1993.

25 S. Havriliak and S. Negami, A Complex Plane Representation of Dielectric and Mechanical Relaxation Processes in Some Polymers, *Polymer*, 1967, **8**(C), 161–210, DOI: 10.1016/0032-3861(67)90021-3.

26 R. Boča and C. Rajnák, Unexpected Behavior of Single Ion Magnets, *Coord. Chem. Rev.*, 2021, **430**, 213657, DOI: 10.1016/j.ccr.2020.213657.

27 S. Stoll and A. Schweiger, EasySpin, a Comprehensive Software Package for Spectral Simulation and Analysis in EPR, *J. Magn. Reson.*, 2006, **178**(1), 42–55, DOI: 10.1016/j.jmr.2005.08.013.

28 M. Suzuki, I. S. Suzuki and J. Walter, Magnetism and superconductivity in $McTa_2S_2C$ (M=Fe, Co, Ni, and Cu), *Phys. Rev. B: Condens. Matter Mater. Phys.*, 2005, **71**(22), 224407, DOI: 10.1103/PhysRevB.71.224407.

29 (*a*) N. Malinová, J. Juráková, B. Brachňaková, J. D. Midlíková, E. Čižmár, V. T. Santana, R. Herchel, M. Orlita, I. Mohelský, J. Moncol, P. Neugebauer and I. Šalitroš, Magnetization Slow Dynamics in Mononuclear Co(II) Field-Induced Single-Molecule Magnet, *Cryst. Growth Des.*, 2023, **23**(4), 2430–2441, DOI: 10.1021/acs.cgd.2c01388; (*b*) J. Juráková, J. Dubnická Midlíková, J. Hrubý, A. Kliuikov, V. T. Santana, J. Pavlik, J. Moncoľ, E. Čižmár, M. Orlita, I. Mohelský, P. Neugebauer, D. Gentili, M. Cavallini and I. Šalitroš, Pentacoordinate Cobalt(II) Single Ion Magnets with Pendant Alkyl Chains: Shall We Go for Chloride or Bromide? Inorg, *Chem. Front.*, 2022, **9**(6), 1179–1194, DOI: 10.1039/D1QI01350E.

30 R. A. D. Wentworth, Trigonal Prismatic vs. Octahedral Stereochemistry in Complexes Derived from Innocent Ligands, *Coord. Chem. Rev.*, 1972, **9**(1–2), 171–187, DOI: 10.1016/S0010-8545(00)80227-1.

31 D. Dai, H. Xiang and M.-H. Whangbo, Effects of Spin-Orbit Coupling on Magnetic Properties of Discrete and Extended Magnetic Systems, *J. Comput. Chem.*, 2008, **29**(13), 2187–2209, DOI: 10.1002/jcc.21011.

32 L. Yan and M.-J. Wang, Synthesis, Crystal Structures and Fluorescence of Two Zn(II) Complexes with Schiff Base Ligands, *Chin. J. Inorg. Chem.*, 2013, **29**(11), 2370–2374, DOI: 10.3969/j.issn.1001-4861.2013.00.351.

33 M. Gruden-Pavlović, M. Perić, M. Zlatar and P. García-Fernández, Theoretical Study of the Magnetic Anisotropy and Magnetic Tunnelling in Mononuclear Ni(Ii) Complexes with Potential Molecular Magnet Behavior, *Chem. Sci.*, 2014, **5**(4), 1453, DOI: 10.1039/c3sc52984c.

34 H.-S. Lv, S.-Y. Huang, Y. Xu, X. Dai, J.-Y. Miao and B.-X. Zhao, A New Fluorescent PH Probe for Imaging Lysosomes in Living Cells, *Bioorg. Med. Chem. Lett.*, 2014, **24**(2), 535–538, DOI: 10.1016/j.bmcl.2013.12.025.

35 (*a*) F. Neese, The ORCA Program System, *Wiley Interdiscip. Rev.: Comput. Mol. Sci.*, 2012, **2**(1), 73–78, DOI: 10.1002/wcms.81; (*b*) F. Neese, Software Update: The ORCA Program System, Version 4.0, *Wiley Interdiscip. Rev.: Comput. Mol. Sci.*, 2018, **8**(1), e1327, DOI: 10.1002/wcms.1327; (*c*) F. Neese, Software Update: The ORCA Program System—Version 5.0, *Wiley Interdiscip. Rev.: Comput. Mol. Sci.*, 2022, **12**(5), e1606, DOI: 10.1002/wcms.1606.

36 A. D. Becke, Density-Functional Exchange-Energy Approximation with Correct Asymptotic Behavior, *Phys. Rev. A*, 1988, **38**(6), 3098–3100, DOI: 10.1103/PhysRevA.38.3098.

37 (*a*) F. Weigend and R. Ahlrichs, Balanced Basis Sets of Split Valence, Triple Zeta Valence and Quadruple Zeta Valence Quality for H to Rn: Design and Assessment of Accuracy, *Phys. Chem. Chem. Phys.*, 2005, **7**(18), 3297–3305, DOI: 10.1039/b508541a; (*b*) F. Weigend, A Fully Direct RI-HF Algorithm: Implementation, Optimised Auxiliary Basis Sets, Demonstration of Accuracy and Efficiency, *Phys. Chem. Chem. Phys.*, 2002, **4**(18), 4285–4291, DOI: 10.1039/b204199p.

38 (*a*) P. J. Stephens, F. J. Devlin, C. F. Chabalowski and M. J. Frisch, Ab Initio Calculation of Vibrational Absorption and Circular Dichroism Spectra Using Density Functional Force Fields, *J. Phys. Chem.*, 1994, **98**(45), 11623–11627, DOI: 10.1021/j100096a001; (*b*) A. D. Becke, Density–functional Thermochemistry. III. The Role of Exact Exchange, *J. Chem. Phys.*, 1993, **98**(7), 5648–5652, DOI: 10.1063/1.464913; (*c*) C. Lee, W. Yang and R. G. Parr, Development of the Colle-Salvetti Correlation-Energy Formula into a Functional of the Electron Density, *Phys. Rev. B: Condens. Matter Mater. Phys.*, 1988, **37**(2), 785–789, DOI: 10.1103/PhysRevB.37.785; (*d*) S. H. Vosko, L. Wilk and M. Nusair, Accurate Spin-Dependent Electron Liquid Correlation Energies for Local Spin Density Calculations: A Critical Analysis, *Can. J. Phys.*, 1980, **58**(8), 1200–1211, DOI: 10.1139/p80-159.

39 E. Caldeweyher, S. Ehlert, A. Hansen, H. Neugebauer, S. Spicher, C. Bannwarth and S. Grimme, A Generally Applicable Atomic-Charge Dependent London Dispersion

Correction, *J. Chem. Phys.*, 2019, **150**(15), 154122, DOI: 10.1063/1.5090222.

40 Y. Guo, K. Sivalingam, E. F. Valeev and F. Neese, Explicitly Correlated N-Electron Valence State Perturbation Theory (NEVPT2-F12), *J. Chem. Phys.*, 2017, **147**(6), 064110, DOI: 10.1063/1.4996560.

41 F. Neese, Efficient and Accurate Approximations to the Molecular Spin-Orbit Coupling Operator and Their Use in Molecular g-Tensor Calculations, *J. Chem. Phys.*, 2005, **122**(3), 034107, DOI: 10.1063/1.1829047.

42 (*a*) L. Ungur, M. Thewissen, J.-P. Costes, W. Wernsdorfer and L. F. Chibotaru, Interplay of Strongly Anisotropic Metal Ions in Magnetic Blocking of Complexes, *Inorg. Chem.*, 2013, **52**(11), 6328–6337, DOI: 10.1021/ic302568x; (*b*) L. F. Chibotaru and L. Ungur, Ab Initio Calculation of Anisotropic Magnetic Properties of Complexes. I. Unique Definition of Pseudospin Hamiltonians and Their Derivation, *J. Chem. Phys.*, 2012, **137**(6), 064112, DOI: 10.1063/1.4739763; (*c*) L. Ungur, W. Van Den Heuvel and L. F. Chibotaru, Ab Initio Investigation of the Non-Collinear Magnetic Structure and the Lowest Magnetic Excitations in Dysprosium Triangles, *New J. Chem.*, 2009, **33**(6), 1224–1230, DOI: 10.1039/b903126j; (*d*) L. F. Chibotaru, L. Ungur and A. Soncini, The Origin of Nonmagnetic Kramers Doublets in the Ground State of Dysprosium Triangles: Evidence for a Toroidal Magnetic Moment, *Angew. Chem., Int. Ed.*, 2008, **47**(22), 4126–4129, DOI: 10.1002/anie.200800283; (*e*) L. F. Chibotaru, L. Ungur, C. Aronica, H. Elmoll, G. Pilet and D. Luneau, Structure, Magnetism, and Theoretical Study of a Mixed-Valence Co II3CoIII4 Heptanuclear Wheel: Lack of SMM Behavior despite Negative Magnetic Anisotropy, *J. Am. Chem. Soc.*, 2008, **130**(37), 12445–12455, DOI: 10.1021/ja8029416; (*f*) L. F. Chibotaru, L. Ungur and A. Soncini, The Origin of Nonmagnetic Kramers Doublets in the Ground State of Dysprosium Triangles: Evidence for a Toroidal Magnetic Moment, *Angew. Chem., Int. Ed.*, 2008, **47**(22), 4126–4129, DOI: 10.1002/anie.200800283.

43 (*a*) A. K. Dutta, F. Neese and R. Izsák, Accelerating the Coupled-Cluster Singles and Doubles Method Using the Chain-of-Sphere Approximation, *Mol. Phys.*, 2018, **116**(11), 1428–1434, DOI: 10.1080/00268976.2017.1416201; (*b*) R. Izsák and F. Neese, An Overlap Fitted Chain of Spheres Exchange Method, *J. Chem. Phys.*, 2011, **135**(14), 144105, DOI: 10.1063/1.3646921; (*c*) F. Neese, F. Wennmohs, A. Hansen and U. Becker, Efficient, Approximate and Parallel Hartree–Fock and Hybrid DFT Calculations. A 'Chain-of-Spheres' Algorithm for the Hartree–Fock Exchange, *Chem. Phys.*, 2009, **356**(1–3), 98–109, DOI: 10.1016/j.chemphys.2008.10.036.

44 M. D. Hanwell, D. E. Curtis, D. C. Lonie, T. Vandermeersch, E. Zurek and G. R. Hutchison, Avogadro: An Advanced Semantic Chemical Editor, Visualization, and Analysis Platform, *J. Cheminf.*, 2012, **4**(1), 17, DOI: 10.1186/1758-2946-4-17.

45 C. F. Macrae, P. R. Edgington, P. McCabe, E. Pidcock, G. P. Shields, R. Taylor, M. Towler and J. van de Streek, Mercury : Visualization and Analysis of Crystal Structures, *J. Appl. Crystallogr.*, 2006, **39**(3), 453–457, DOI: 10.1107/S002188980600731X.

46 N. F. Chilton, R. P. Anderson, L. D. Turner, A. Soncini and K. S. Murray, PHI: A Powerful New Program for the Analysis of Anisotropic Monomeric and Exchange-Coupled Polynuclear d - and f -Block Complexes, *J. Comput. Chem.*, 2013, **34**(13), 1164–1175, DOI: 10.1002/jcc.23234.

47 M. Liberka, M. Zychowicz, W. Zychowicz and S. Chorazy, Neutral Dicyanidoferrate(ii) Metalloligands for the Rational Design of Dysprosium(III) Single-Molecule Magnets, *Chem. Commun.*, 2022, **58**(44), 6381–6384, DOI: 10.1039/D2CC02238A.

48 OpenAI ChatGPT (2023). https://chat.openai.com/. *ChatGPT 12 May version*.